

Stiffness characterization of a 3-PPR planar parallel manipulator with actuation compliance

Proc IMechE Part C:

J Mechanical Engineering Science

2015, Vol. 229(12) 2291–2302

© IMechE 2014

Reprints and permissions:

sagepub.co.uk/journalsPermissions.nav

DOI: 10.1177/0954406214557341

pic.sagepub.com

Guanglei Wu, Shaoping Bai and Jørgen Kepler

Abstract

This paper investigates the stiffness of a compliant planar parallel manipulator. Instead of establishing stiffness matrix directly for planar mechanisms, we adopt the modeling approach for spatial mechanisms, which allows us to derive two decoupled homogeneous matrices, corresponding to the translational and rotational stiffness. This is achieved by resorting to the generalized eigenvalue problem, through which the eigenscrew decomposition is implemented to yield six screw springs. The principal stiffnesses and their directions are then identified from the eigenvalue problem of the two separated submatrices. In addition, the influence of the nonlinear actuation compliance to the manipulator stiffness is investigated, and the established stiffness model is experimentally verified.

Keywords

Planar parallel manipulators, actuation compliance, eigenscrew decomposition, eigenforce, stiffness decoupling

Date received: 7 March 2014; accepted: 6 October 2014

Introduction

The planar parallel manipulators (PPMs) have found their applications in many fields. Their stiffness is one of the important considerations in design and applications in that the stiffness decides the positioning and orientation accuracies. In some applications, such as the Remote Center Compliance (RCC) device,¹ which allows multi-axis movement to achieve lateral and angular alignment between components, the conventional stiffness formulation corresponding to their mobilities cannot characterize the stiffness precisely, thus, stiffness modeling with increased dimensions for PPMs is desirable.

The stiffness matrix of a mechanism maps the transformation between the translational/rotational deformation and the external wrench applied. A number of works on the stiffness of the compliant PPMs can be found in the literature. Kim et al.² analyzed the output compliance characteristics of a completely decoupled 3-RRR PPM as a Remote Center of Compliance (RCC) device. Kock and Schumacher³ investigated a two degrees-of-freedom (2-dof) planar manipulator with redundant actuation, allowing adjustment towards improved overall stiffness isotropy over the workspace. Similarly, Lee et al.⁴

proposed a method of the equal minimum and maximum stiffness for a 2-DOF PPM by adding redundant actuation. Zhao et al.⁵ investigated the influence of the external force on the stiffness performance of planar parallel 3-RRR mechanism with flexible joints. Besides, the stiffness of the flexure-based PPMs was extensively investigated by several researchers.^{6–10} As frequently documented, the stiffness matrix of parallel robots is usually configuration-dependent and related to the stiffness of joints, linkages and actuators. In this work, these elements and the nonlinear actuation compliance are taken into account to model the stiffness matrix for PPMs.

On the analysis of the manipulator stiffness, a problem usually encountered is that the stiffness matrix is usually dimensionally inhomogeneous, which does not admit a norm to evaluate the manipulator stiffness. Ciblak and Lipkin¹¹ used screw algebra

Department of Mechanical and Manufacturing Engineering, Aalborg University, Aalborg, Denmark

Corresponding author:

Guanglei Wu, Department of Mechanical and Manufacturing Engineering, Aalborg University, DK-9220 Aalborg, Denmark.
Email: gwu@m-tech.aau.dk; glwu0115@gmail.com

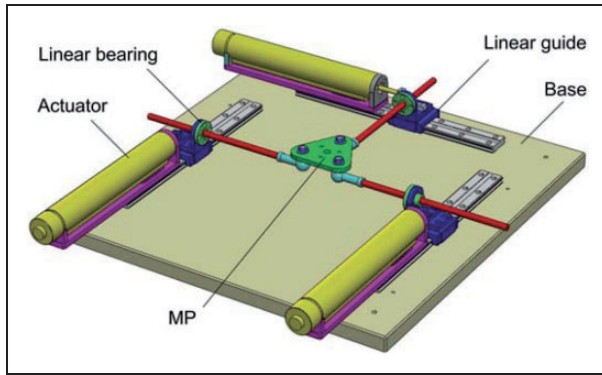


Figure 1. CAD model of an unsymmetrical 3-PPR PPM.

to synthesize a linearly elastic suspension composed of simple translational springs with a prescribed stiffness matrix. Ding and Selig¹² used a finite element model to compute the Cartesian stiffness matrix of a coiled spring, being a more general suspension, which leads to a natural mechanical interpretation of the eigenvalues and eigenvectors of the stiffness matrix. Dai and Ding¹³ derived compliance matrix of a three-legged rigidly-connected platform as a congruence transformation of the legs' compliance matrices and analyzed the compliance characteristics based on the eigencompliances and eigentwist decomposition of the compliance matrix. Kövecses and Ebrahimi¹⁴ proposed a decomposition of the dynamic inertia matrix by changing variables to make the matrix homogeneous, which can be applied to the stiffness matrix.¹⁵ Based on the screw theory, Angeles¹⁶ discussed decoupling and decomposition of the 6×6 Cartesian stiffness matrix. Henceforth, this approach will be used to investigate the stiffness properties of PPMs.

In this paper, the Cartesian stiffness matrix of the PPMs is modeled and analyzed by resorting the modeling approach of spatial mechanisms, in combination with consideration of actuation compliance. The stiffness characteristics is analyzed and discussed by eigenscrew decomposition and decoupling of the Cartesian stiffness matrix, through which the principal stiffnesses and their directions are identified. This approach was applied to a partly decoupled 3-PPR PPM^{17,18} as shown in Figure 1. The influence of the nonlinear actuation compliance was investigated and experimentally verified.

Stiffness modeling of the PPM

A general 3-PPR PPM is illustrated in Figure 2, where A_i , $i = 1, 2, 3$, are points on the base platform and where D_i , $i = 1, 2, 3$, are the points on the moving platform (MP). Frame \mathcal{F}_b is the global coordinate system while \mathcal{F}_p is a moving coordinate system with the origin P located at the geometric center of the moving platform and the X -axis is parallel to the segment D_1D_2 .

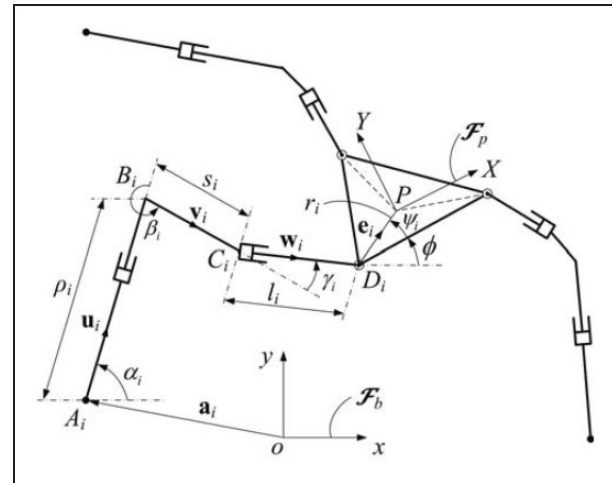


Figure 2. Parameterization of a general kinematic 3-PPR PPM.

The pose of the MP is described by $\mathbf{x} = [\mathbf{p}, \phi]^T$, where $\mathbf{p} = [x, y]^T$.

The stiffness model is established with the virtual-spring approach¹⁹ based on the screw coordinates,²⁰ the flexibility of the i th leg being represented in Figure 3, of which the passive prismatic joint is equivalent to a cylindrical one with the consideration of the MP twist.

Let the MP center be the reference point, the Cartesian stiffness matrix \mathbf{K}_i of the i th leg is obtained by extracting the first six-dimensional block from the following matrix \mathbf{K}'_i , namely,

$$\mathbf{K}'_i = \begin{bmatrix} \mathbf{J}_\rho^i(K_{act}^i)^{-1}\mathbf{J}_\rho^{i^T} + \mathbf{J}_\theta^i(K_\theta^i)^{-1}\mathbf{J}_\theta^{i^T} & \mathbf{J}_q^i \\ \mathbf{J}_q^{iT} & \mathbf{0}_3 \end{bmatrix}^{-1} \quad (1)$$

where \mathbf{J}_ρ^i and \mathbf{J}_θ^i describe the displacements of the actuated joint and the articulated joints relative to the MP center, and \mathbf{J}_q^i takes into account the passive-joint influence on the MP motions, of which the expressions are given in Appendix. Moreover, K_{act}^i describes the actuation stiffness of the i th actuator, and 21×21 matrix \mathbf{K}_θ^i describes the stiffness of all virtual springs, taking the form:

$$\mathbf{K}_\theta^i = \text{diag} \left[\mathbf{K}_g^i \quad \mathbf{K}_s^i \quad \mathbf{K}_b^i \quad \mathbf{K}_{s(l)}^i \right] \quad (2)$$

where \mathbf{K}_g^i , \mathbf{K}_b^i and $\mathbf{K}_{s(l)}^i$, respectively, are the stiffness matrices of the linear guide, bearing and the proximal (distal) link, which take the form:

$$\mathbf{K}_g^i = \text{diag} [k_{\phi x} \quad k_{\phi y} \quad k_{\phi z} \quad k_{yy} \quad k_{zz}]_g^i \quad (3a)$$

$$\mathbf{K}_b^i = \text{diag} [k_{\phi y} \quad k_{\phi z} \quad k_{yy} \quad k_{zz}]_b^i \quad (3b)$$

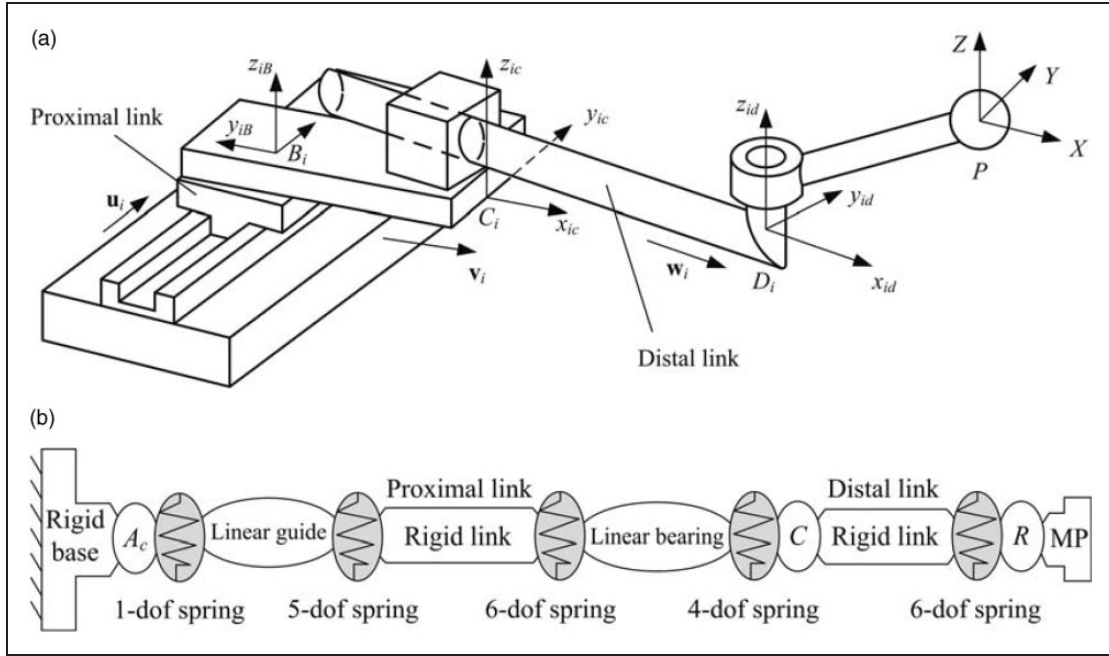


Figure 3. A single flexible leg: (a) a PPR leg with local frames; (b) virtual-spring model, where A_c stands for the actuator, C and R for cylindrical and revolute joints, respectively.

$$\mathbf{K}_{s(l)}^i = \begin{bmatrix} \frac{L}{GI_x} & 0 & 0 & 0 & 0 & 0 \\ 0 & \frac{L}{EI_y} & 0 & 0 & 0 & -\frac{L^2}{2EI_y} \\ 0 & 0 & \frac{L}{EI_z} & 0 & \frac{L^2}{2EI_z} & 0 \\ 0 & 0 & 0 & \frac{L}{EA} & 0 & 0 \\ 0 & 0 & \frac{L^2}{2EI_z} & 0 & \frac{L^3}{3EI_z} & 0 \\ 0 & -\frac{L^2}{2EI_y} & 0 & 0 & 0 & \frac{L^3}{3EI_y} \end{bmatrix}_{s(l)}^i \quad (3c)$$

where L is the link length, A is its cross-section area, $I_y(I_z)$, and I_x are the quadratic and polar moments of inertia of the crosssection, and E and G are the Young's and shear modules, respectively. Moreover, $k_{\phi\epsilon}$ and $k_{\epsilon\epsilon}$, $\epsilon \in \{x, y, z\}$, stand for the rotational and translational stiffnesses in the ϵ direction, respectively.

Henceforth, the Cartesian stiffness matrix \mathbf{K} of the system is found by simple addition, namely,

$$\mathbf{K} = \sum_{i=1}^3 \mathbf{K}_i \quad (4)$$

Eigenscrew decomposition of the stiffness matrix

To characterize the manipulator stiffness at a given configuration, the eigenscrew decomposition is applied to the Cartesian stiffness matrix. For the principal screws of the potential,²¹ the twist and the

wrench have the same line of action and the same pitch. In essence, the principal screws are the eigenvectors ζ_i , of the generalized eigenvalue problem,

$$\mathbf{K}\zeta_i = \lambda_i \Gamma \zeta_i \quad (5)$$

where Γ is the 6×6 permutation matrix defined in its block form

$$\Gamma = \begin{bmatrix} \mathbf{0}_3 & \mathbf{1}_3 \\ \mathbf{1}_3 & \mathbf{0}_3 \end{bmatrix} \quad (6)$$

In screw theory, the corresponding pitch p_i , unit vector \mathbf{e}_i and position vector \mathbf{p}_i of the eigenscrew upon which the eigenforce¹⁶ κ_i acted are defined as below

$$\kappa_i \begin{bmatrix} \mathbf{e}_i \\ \mathbf{p}_i + p_i \mathbf{e}_i \end{bmatrix} = \lambda_i \begin{bmatrix} \boldsymbol{\eta}_i \\ \boldsymbol{\xi}_i \end{bmatrix} \quad (7)$$

where $\boldsymbol{\eta}_i$ and $\boldsymbol{\xi}_i$ are three-dimensional vectors in eigenvector ζ_i . Thus, the eigenforce is calculated as

$$\kappa_i = \lambda_i \|\boldsymbol{\eta}_i\| \quad (8)$$

whence, the unit vector in the eigenscrew is computed from

$$\mathbf{e}_i = \frac{\boldsymbol{\eta}_i}{\|\boldsymbol{\eta}_i\|} \quad (9)$$

and the position vector and eigenpitch will be

$$\mathbf{p}_i = \frac{\boldsymbol{\eta}_i \times \boldsymbol{\xi}_i}{\|\boldsymbol{\eta}_i\|^2} \quad (10)$$

$$p_i = \frac{\boldsymbol{\eta}_i^T \boldsymbol{\xi}_i}{\|\boldsymbol{\eta}_i\|^2} \quad (11)$$

The physical interpretation of stiffness matrix \mathbf{K} can be described by a body supported by six screw springs with directions along their corresponding eigenscrews. Each screw spring is defined by its spring constant $k = \lambda/(2p)$,²² axis direction \mathbf{e} , position vector \mathbf{p} and pitch p .

Decoupling of the stiffness matrix

The stiffness matrix of equation (4) is in general form

$$\mathbf{K} = \begin{bmatrix} \mathbf{K}_{rr} & \mathbf{K}_{rt} \\ \mathbf{K}_{rt}^T & \mathbf{K}_{tt} \end{bmatrix} \quad (12)$$

Decoupling of the Cartesian stiffness matrix is possible if and only if the 3×3 coupling entry \mathbf{K}_{rt} is singular,¹⁶ namely, $\text{rank}(\mathbf{K}_{rt}) \leq 2$, which is achieved by means of a similarity transformation that involves only a shift of the origin. In general, \mathbf{K}_{rt} is not singular for the spatial case, but becomes singular for planar case when considered in 3D space.

Let the stiffness matrix under study be denoted by $[\mathbf{K}]_{\mathcal{A}}$ when represented in a coordinate frame labeled by \mathcal{A} . Similarly, $[\mathbf{K}]_{\mathcal{B}}$ stands for the same matrix in a second frame \mathcal{B} , under the assumption that the orientation of the axes and origins of the two frames are different. The matrix \mathbf{T} transforms a unit screw $\hat{\mathbf{s}}$ from \mathcal{B} into \mathcal{A} given by²³

$$[\hat{\mathbf{s}}]_{\mathcal{B}} = \mathbf{T}[\hat{\mathbf{s}}]_{\mathcal{A}}; \quad \mathbf{T} = \begin{bmatrix} \mathbf{Q} & \mathbf{0}_3 \\ \mathbf{D}\mathbf{Q} & \mathbf{Q} \end{bmatrix} \quad (13)$$

where \mathbf{Q} denotes the rotation matrix from the frame \mathcal{B} to \mathcal{A} , while \mathbf{D} is the cross-product matrix (CPM) of the displacement \mathbf{d} that carries the origin of frame \mathcal{B} into that of \mathcal{A} , defined as $\mathbf{D} = \text{CPM}(\mathbf{d})$.²⁴ The corresponding changes in axis-coordinates $\hat{\mathbf{s}}_a$ are done by

$$[\hat{\mathbf{s}}_a]_{\mathcal{B}} = \Gamma[\hat{\mathbf{s}}]_{\mathcal{B}} = \Gamma\mathbf{T}[\hat{\mathbf{s}}]_{\mathcal{A}} = \Gamma\mathbf{T}\Gamma^{-1}[\hat{\mathbf{s}}_a]_{\mathcal{A}} \quad (14)$$

The matrices $[\mathbf{K}]_{\mathcal{A}}$ and $[\mathbf{K}]_{\mathcal{B}}$ are displayed below:

$$[\mathbf{K}]_{\mathcal{A}} = \begin{bmatrix} \mathbf{K}_{rr} & \mathbf{K}_{rt} \\ \mathbf{K}_{rt}^T & \mathbf{K}_{tt} \end{bmatrix}; \quad [\mathbf{K}]_{\mathcal{B}} = \begin{bmatrix} \mathbf{K}'_{rr} & \mathbf{K}'_{rt} \\ \mathbf{K}'_{rt}^T & \mathbf{K}'_{tt} \end{bmatrix} \quad (15)$$

In light of the definition equation (14), the similarity transformation that relates $[\mathbf{K}]_{\mathcal{A}}$ with $[\mathbf{K}]_{\mathcal{B}}$ is²⁵

$$\begin{aligned} [\mathbf{K}]_{\mathcal{B}} &= \Gamma\mathbf{T}\Gamma^{-1}[\mathbf{K}]_{\mathcal{A}}\mathbf{T}^{-1}; \\ \Gamma\mathbf{T}\Gamma^{-1} &= \Gamma\mathbf{T}\Gamma = \begin{bmatrix} \mathbf{Q} & \mathbf{D}\mathbf{Q} \\ \mathbf{0}_3 & \mathbf{Q} \end{bmatrix} \end{aligned} \quad (16)$$

Combining equations (15) and (16) leads to

$$\mathbf{K}'_{rr} = \mathbf{Q}(\mathbf{K}_{rr} - \mathbf{K}_{rt}\mathbf{D})\mathbf{Q}^T + \mathbf{D}\mathbf{Q}(\mathbf{K}_{rt}^T - \mathbf{K}_{tt}\mathbf{D})\mathbf{Q}^T \quad (17a)$$

$$\mathbf{K}'_{rt} = (\mathbf{Q}\mathbf{K}_{rt} + \mathbf{D}\mathbf{Q}\mathbf{K}_{tt})\mathbf{Q}^T \quad (17b)$$

$$\mathbf{K}'_{tt} = \mathbf{Q}\mathbf{K}_{tt}\mathbf{Q}^T \quad (17c)$$

As matrix \mathbf{Q} can be freely chosen, to meet the decoupling condition $\mathbf{K}'_{rt} = \mathbf{0}_3$, we can let $\mathbf{Q} = \mathbf{1}$, which yields

$$\mathbf{K}'_{rr} = \mathbf{K}_{rr} - \mathbf{K}_{rt}\mathbf{D} + \mathbf{D}(\mathbf{K}_{rt}^T - \mathbf{K}_{tt}\mathbf{D}) \quad (18a)$$

$$\mathbf{D}\mathbf{K}_{tt} = -\mathbf{K}_{rt} \quad (18b)$$

$$\mathbf{K}'_{tt} = \mathbf{K}_{tt} \quad (18c)$$

whence \mathbf{D} can be determined from equation (18b), being a 3×3 skew-symmetric matrix, hence, $\text{rank}(\mathbf{D}\mathbf{K}_{tt}) \leq 2$, in accordance with Sylvester's theorem.²⁶ Under the assumption that \mathbf{K}_{rt} is singular, \mathbf{D} is found upon taking the axial vector²⁴ of both sides of equation (18b), namely,

$$\mathbf{M}\mathbf{d} = \text{vect}(\mathbf{K}_{rt}); \quad \mathbf{M} = \frac{1}{2}[1\text{tr}(\mathbf{K}_{tt}) - \mathbf{K}_{tt}] \quad (19)$$

where \mathbf{M} carries unit N/m and $\text{tr}(\mathbf{K}_{tt})$ is the trace of \mathbf{K}_{tt} . Operation $\text{vect}(\cdot)$ is the mapping from anti-screw matrix to its corresponding vector. If \mathbf{M} is invertible, then $\mathbf{d} = \mathbf{M}^{-1}\text{vect}(\mathbf{K}_{rt})$; otherwise, \mathbf{M} fails to be invertible, but \mathbf{d} can still be calculated.¹⁶

Actuator stiffness

In some developed stiffness models, actuator stiffness is usually considered as constant when the transmission unit is mechanically locked. However, in real applications, where actuator is powered, the actuation stiffness may change and influence the overall stiffness significantly. For the PPM in this work, SMAC actuators are moving coil linear motors driven by electromagnetic force, which behaves similarly as the compression/tension spring, hence, their stiffness strongly influences the manipulator stiffness. The actuator stiffness K_{act}^i is modeled from static-load experiment when the actuator is powered on, for which the experimental setup is shown in Figure 4(a).

The force-displacement curve is shown in Figure 4(b), from which it is seen that measurements of applied force versus extension of actuator rod do not obey Hooke's Law, but display as a nonlinear softening spring. The force-displacement curve is in this case fitted into an exponential function as

$$G = k_a \delta_a^q \quad (20)$$

where $k_a = 44.75$ is the generalized actuation stiffness with unit of N/m^q, and the exponent $q = 0.225$ describes how much the stiffness changes with force.²⁷ A greater value of q means a greater range of stiffness for a given range of force. Equation (20)

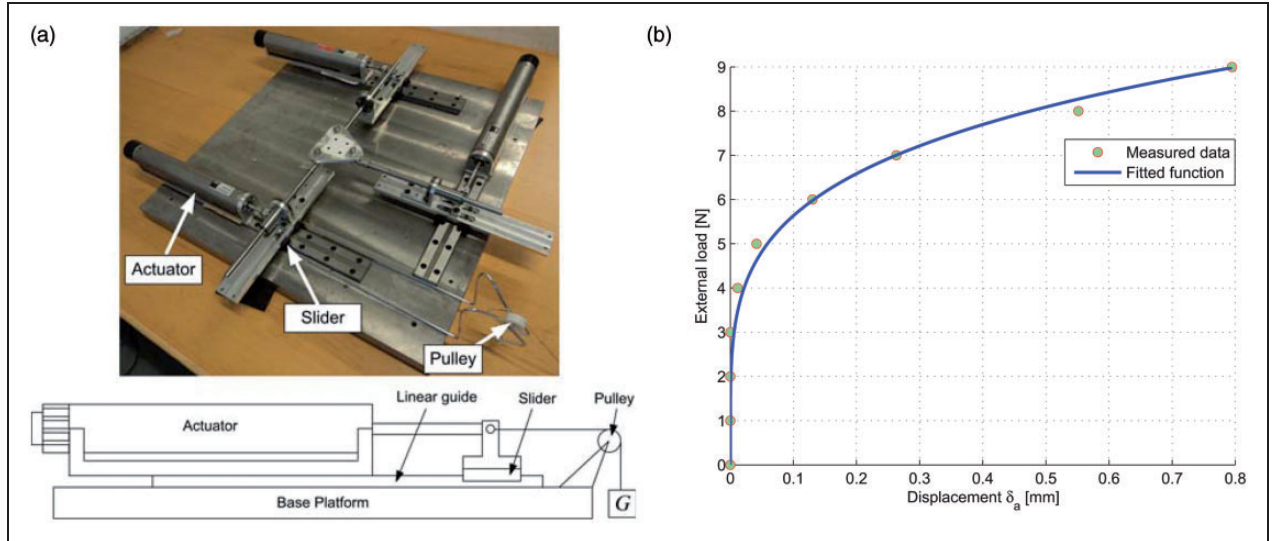


Figure 4. Static load experiment of the actuator: (a) setup, (b) force–displacement curve.

becomes linear when $q=1$. The actuator behaves different stiffness characteristics due to the nonlinear displacements under different external loads applied to the actuator rod. With consideration of friction introduced by the sliding unit and linear guide, the actuator stiffness is expressed as

$$K_{\text{act}}^i = \begin{cases} 1.1108 \cdot 10^5 \text{ N/m}, & \delta_a \leq 0.006 \text{ mm} \\ qk_a \delta_{ai}^{q-1}, & \delta_{ai} > 0.006 \text{ mm}, i = 1, 2, 3 \end{cases} \quad (21)$$

Stiffness Performance of the 3-PPR PPM

In this section, the decoupling of the stiffness matrix is applied to the 3-PPR PPM in Figure 1. The foregoing analysis based on screw theory is employed to find the eigenscrews and principal stiffnesses of the Cartesian stiffness matrix to characterize the stiffness properties.

Analysis of the stiffness matrix

The design parameters are given in Table 1 and $\gamma_i=0$, $r_i=30$ mm. Moreover, the kinematic problem of the PPM has been well documented in the previous work.¹⁸ The material properties and element stiffnesses are listed in Tables 2 and 3, respectively. When the manipulator is at its workspace center with $\phi=0$, the stiffness matrix of unloaded mode is computed as

$$\mathbf{K} = \begin{bmatrix} \mathbf{K}_{rr} & \mathbf{K}_{rt} \\ \mathbf{K}_{rt}^T & \mathbf{K}_{tt} \end{bmatrix} = \begin{bmatrix} 0.0075 & 0.0006 & 0 & 0 & 0 & 0.0323 \\ 0.0006 & 0.0143 & 0 & 0 & 0 & -0.0398 \\ 0 & 0 & 0.0008 & -0.0104 & 0.0043 & 0 \\ 0 & 0 & -0.0104 & 0.3457 & 0 & 0 \\ 0 & 0 & 0.0043 & 0 & 0.6595 & 0 \\ 0.0323 & -0.0398 & 0 & 0 & 0 & 1.4229 \end{bmatrix} \cdot 10^5 \quad (22)$$

Table 1. The design parameters of the 3-PPR PPM.

i	a_i (mm)	α_i (rad)	β_i (rad)	ψ_i (rad)	s_i (mm)
1	(-179.97, -67.86)	$\pi/2$	$-\pi/2$	$\pi/6$	114
2	(179.97, -67.86)	$\pi/2$	$\pi/2$	$5\pi/6$	27
3	(-34.47, 189.23)	0	$-\pi/2$	$3\pi/2$	42

where the blocks \mathbf{K}_{rr} , \mathbf{K}_{rt} and \mathbf{K}_{tt} are given in Nm, N and N/m, respectively. The block \mathbf{K}_{tt} becomes a diagonal matrix due to the partly decoupled mobilities in x - and y -axis. With external forces $\mathbf{f}=[f_{xy}, f_z]^T$ and/or moments m_z acting on the mobile platform, where $f_{xy}=f_{xy}[\cos \alpha, \sin \alpha]$, the deflections can be calculated from the compliance matrix, i.e., the inverse of matrix (22).

Solutions of the generalized eigenvalue problem. Solving the generalized eigenvalue problem of matrix (22), the eigenstiffnesses (eigenvalues) and their corresponding eigenvectors are listed as follow

$$\lambda = [9624.4 \ 4759.3 \ 2368.1 \ -9624.4 \ -4759.3 \ -2368.1]^T \quad (23)$$

Table 2. Properties of the proximal and distal links.

	E (Gpa)	G (Gpa)	A (m^2)	I_x (m^4)	I_y (m^4)	I_z (m^4)
Proximal	69	26	$2.1 \cdot 10^{-4}$	$2.21 \cdot 10^{-8}$	$6.30 \cdot 10^{-10}$	$2.14 \cdot 10^{-8}$
Distal	210	81	$5.03 \cdot 10^{-5}$	$4.02 \cdot 10^{-10}$	$2.01 \cdot 10^{-10}$	$2.01 \cdot 10^{-10}$

Table 3. The elements of the stiffness matrix of the linear guide and bearing.

Linear guide			Linear bearing		
k_{ϕ_x} (Nm/rad)	k_{ϕ_y}, k_{ϕ_z} (Nm/rad)	k_{yy} (N/m)	k_{zz} (N/m)	k_{ϕ_y}, k_{ϕ_z} (Nm/rad)	k_{yy}, k_{zz} (N/m)
4700	1700	$2.5 \cdot 10^6$	$5.1 \cdot 10^6$	1010	$1.996 \cdot 10^6$

Table 4. Details of the screw springs.

Spring	k (N/m)	\mathbf{e}	\mathbf{p} (m)	p (rad/m)
s1	36602	$[0.0820, 0.9408, -0.3289]^T$	$[0.0479, -0.0044, -0.0008]^T$	0.1315
s2	17866	$[0.9757, -0.1653, -0.1437]^T$	$[0.0036, 0.0122, 0.0108]^T$	0.1332
s3	66947	$[0.0223, 0.0385, 0.9990]^T$	$[0.0057, 0.0311, -0.0013]^T$	0.0177
s4	36602	$[0.0820, 0.9408, 0.3289]^T$	$[0.0479, -0.0044, -0.0008]^T$	-0.1315
s5	17866	$[0.9757, -0.1653, 0.1437]^T$	$[0.0036, 0.0122, -0.0108]^T$	-0.1332
s6	66947	$[-0.0223, -0.0385, 0.9990]^T$	$[0.0057, 0.0311, 0.0013]^T$	-0.0177

and the eigenscrews are found as

$$\Lambda = [\Lambda_1 \ \Lambda_2]; \quad \Lambda_1 = \begin{bmatrix} 0.0812 & 0.9671 & 0.0222 \\ 0.9317 & -0.1638 & 0.0385 \\ -0.3258 & -0.1424 & 0.9984 \\ 0.0128 & 0.1288 & 0.0315 \\ 0.1381 & -0.0109 & -0.0051 \\ 0.0022 & -0.0313 & 0.0172 \end{bmatrix}, \quad (24)$$

$$\Lambda_2 = \begin{bmatrix} 0.0812 & 0.9671 & -0.0222 \\ 0.9317 & -0.1638 & -0.0385 \\ 0.3258 & 0.1424 & 0.9984 \\ -0.0128 & -0.1288 & 0.0315 \\ -0.1381 & 0.0109 & -0.0051 \\ 0.0022 & -0.0313 & -0.0172 \end{bmatrix}$$

$$\mathbf{S} = [\mathbf{S}_1 \ \mathbf{S}_2], \quad \mathbf{S}_1 = \begin{bmatrix} 0.0820 & 0.9757 & 0.0223 \\ 0.9408 & -0.1653 & 0.0385 \\ -0.3290 & -0.1437 & 0.9990 \\ 0.0130 & 0.1300 & 0.0315 \\ 0.1394 & -0.0110 & -0.0051 \\ 0.0022 & -0.0316 & 0.0172 \end{bmatrix}, \quad (27)$$

$$\mathbf{S}_2 = \begin{bmatrix} 0.0820 & 0.9757 & -0.0223 \\ 0.9408 & -0.1653 & -0.0385 \\ 0.3290 & 0.1437 & 0.9990 \\ -0.0130 & -0.1300 & 0.0315 \\ -0.1394 & 0.0110 & -0.0051 \\ 0.0022 & -0.0316 & -0.0172 \end{bmatrix}$$

whereby the six eigenforces are obtained pairwisely as

$$\kappa_1 = -\kappa_4 = 9531.5 \text{ N}; \quad \kappa_2 = -\kappa_5 = 4717.0 \text{ N};$$

$$\kappa_3 = -\kappa_6 = 2366.6 \text{ N} \quad (25)$$

and the associated eigenpitches being

$$p_1 = -p_4 = 0.1315 \text{ rad/m};$$

$$p_2 = -p_5 = 0.1332 \text{ rad/m}; \quad (26)$$

$$p_3 = -p_6 = 0.0177 \text{ rad/m}$$

The smaller eigenforce implies that the manipulator is stiffer in this direction.¹⁶ The physical interpretation of stiffness matrix (22) is listed in Table 4 and graphically shown in Figure 5.

Principal stiffnesses and directions. Apparently, the rank of \mathbf{K}_{rt} in matrix (22) is equal to 2, thus, \mathbf{K} can be decoupled. Matrix \mathbf{M} in equation (19) is computed as

$$\mathbf{M} = \begin{bmatrix} 1.0413 & 0 & 0 \\ 0 & 0.8843 & 0 \\ 0 & 0 & 0.5027 \end{bmatrix} \cdot 10^5 \text{ N/m} \quad (28)$$

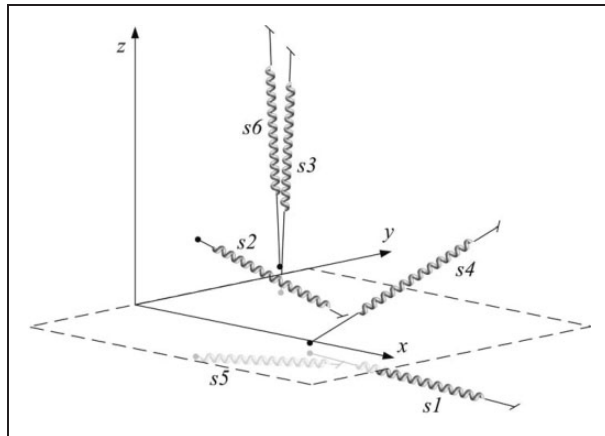


Figure 5. Physical interpretation of stiffness matrix with six screw springs.

which is invertible, consequently, \mathbf{d} follows the simple inversion of \mathbf{M}

$$\mathbf{d} = [0.0212 \quad 0.0241 \quad 0]^T \text{ m} \quad (29)$$

Following the relation $\mathbf{D} = \text{CPM}(\mathbf{d})$, one obtains

$$\mathbf{D} = \begin{bmatrix} 0 & 0 & 0.0241 \\ 0 & 0 & -0.0212 \\ -0.0241 & 0.0212 & 0 \end{bmatrix} \text{ m} \quad (30)$$

Substituting matrix \mathbf{D} into equations (18a) and (18c), \mathbf{K}'_{rr} and \mathbf{K}'_{tt} are calculated as

$$\mathbf{K}'_{rr} = \begin{bmatrix} 0.9880 & -0.1776 & 0 \\ -0.1776 & 1.6624 & 0 \\ 0 & 0 & 0.1935 \end{bmatrix} \cdot 10^3 \text{ Nm};$$

$$\mathbf{K}'_{tt} = \begin{bmatrix} 0.3458 & 0 & 0 \\ 0 & 0.6597 & 0 \\ 0 & 0 & 1.4229 \end{bmatrix} \cdot 10^5 \text{ N/m} \quad (31)$$

Matrix \mathbf{K} is decoupled into two homogeneous sub-matrices corresponding to the translational and rotational stiffness, thus, by addressing the simple

$$\mathbf{K} = \begin{bmatrix} 0.0075 & 0.0006 & 0 & 0 & 0 \\ 0.0006 & 0.0143 & 0 & 0 & 0 \\ 0 & 0 & 0.0003 & -0.0042 & -0.0052 \\ 0 & 0 & -0.0042 & 0.1385 & 0 \\ 0 & 0 & -0.0052 & 0 & 0.2954 \\ 0.0323 & -0.0398 & 0 & 0 & 0 \end{bmatrix} \cdot 10^5 \quad (32)$$

eigenvalue problem, one can identify the directions along which the max-/minimum principal stiffness exists. Based on this, the corresponding eigenvalues and eigenvectors of \mathbf{K}'_{rr} (\mathbf{K}'_{tt}), stored in arrays \mathbf{f}_{rr} (\mathbf{f}_{tt}) and matrices $\mathbf{\Lambda}_{rr}$ ($\mathbf{\Lambda}_{tt}$), respectively, are displayed below

$$\mathbf{f}_{rr} = \begin{bmatrix} 0.9441 \\ 1.7063 \\ 0.1935 \end{bmatrix} \cdot 10^3 \text{ Nm}, \quad \mathbf{\Lambda}_{rr} = \begin{bmatrix} -0.9708 & 0.2400 \\ -0.2400 & -0.9708 \\ 0 & 0 \end{bmatrix}$$

It is noteworthy that the manipulator has the largest translational stiffness but the smallest rotational stiffness in the z -axis, since the resistance to the linear deformation in this direction depends only on the structural stiffness which is much larger than the actuation stiffness, whereas the rotational stiffness mainly comes from the actuator at a prescribed configuration. With the partly decoupled characteristics, the second eigenvalue in \mathbf{f}_{rr} is approximately twice as large as the first one and so is \mathbf{f}_{tt} . In addition, the identity matrix $\mathbf{\Lambda}_{tt}$ indicates that the principal directions of translational stiffness are parallel to the global coordinate axes regardless of the manipulator pose.

Reference to the mobilities of the planar manipulators, the principal stiffness, i.e., the third eigenvalue in \mathbf{f}_{rr} and the first two ones in \mathbf{f}_{tt} , denoted by k_ϕ , k_x and k_y , respectively, should be given due attention. The larger the eigenvalues, the stiffer the manipulator. The eigenvectors of the force demonstrate the compliant directions in the xy plane. As the stiffness analysis plays a significant role in the manipulator design, the decoupling of stiffness matrix can be applied in this process, through which parameters and dimensions are evaluated to optimize the manipulator performance.

Actuation compliance effect on manipulator stiffness

The actuator stiffness in equation (1) has a much more significant influence on the overall compliance than the structural stiffness. Thereby, the effect of structural stiffness variation due to geometry changes may be ignored when an external wrench is applied to the MP. When the manipulator is still at its workspace center with $\phi = 0$ but under an external wrench $\mathbf{w}_e = [\mathbf{f}^T \, m_z]^T$, where $\mathbf{f} = [5, 5, 20]^T \text{ N}$ and $m_z = 0.1 \text{ Nm}$, the actuation stiffnesses are $K_{\text{act}}^1 = 1.1108 \cdot 10^5 \text{ N/m}$, $K_{\text{act}}^2 = 0.0516 \cdot 10^5 \text{ N/m}$, $K_{\text{act}}^3 = 0.1912 \cdot 10^5 \text{ N/m}$, leading to the stiffness matrix

$$\begin{bmatrix} 0.0323 \\ -0.0398 \\ 0 \\ 0 \\ 0 \end{bmatrix} \cdot 10^5 \quad (33)$$

By comparison, it is found that part of the elements are different from matrix (22), as the actuation stiffness can only contribute to affect the elements corresponding to the stiffness matrix in its planar version. Henceforth, the eigenforces,

$$\begin{bmatrix} 0 \\ 0 \\ 1 \end{bmatrix}; \quad \mathbf{f}_{tt} = \begin{bmatrix} 0.3458 \\ 0.6597 \\ 1.4229 \end{bmatrix} \cdot 10^5 \text{ N/m}, \quad \mathbf{\Lambda}_{tt} = \begin{bmatrix} 1 & 0 & 0 \\ 0 & 1 & 0 \\ 0 & 0 & 1 \end{bmatrix} \quad (32)$$

eigenpitches and eigenscrews, respectively, are found as below

$$\begin{aligned}\kappa_1 &= -\kappa_4 = 6871.4 \text{ N}; \quad \kappa_2 = -\kappa_5 = 2939.4 \text{ N}; \\ \kappa_3 &= -\kappa_6 = 1117.7 \text{ N}\end{aligned}\quad (34a)$$

$$\begin{aligned}p_1 &= -p_4 = 0.1227 \text{ rad/m}; \\ p_2 &= -p_5 = 0.2145 \text{ rad/m}; \\ p_3 &= -p_6 = 0.0097 \text{ rad/m}\end{aligned}\quad (34b)$$

$$\mathbf{S} = \left[\begin{array}{c|ccccc} -0.0506 & -0.9885 & 0.0038 & 0.0506 & 0.9885 & 0.0038 \\ -0.7158 & 0.1495 & 0.0394 & 0.7158 & -0.1495 & 0.0394 \\ 0.6965 & 0.0218 & 0.9992 & 0.6965 & 0.0218 & -0.9992 \\ -0.0045 & -0.2140 & 0.0303 & -0.0045 & -0.2140 & -0.0303 \\ -0.1563 & 0.0156 & 0.0190 & -0.1563 & 0.0156 & -0.0190 \\ 0.0152 & 0.0271 & 0.0089 & -0.0152 & -0.0271 & 0.0089 \end{array} \right] \quad (34c)$$

The corresponding physical interpretation of stiffness matrix under external forces/moment is listed in Table 5, from which it is seen that the directions of the third pair of springs do not have obvious change compared to Table 4, which are still approximately parallel to the z -axis. It is noted that the magnitudes of all the eigenforces and the spring constants become smaller with the decreased diagonal elements.

Solving the eigenvalue problem based on the decoupling of the stiffness matrix, the principal stiffnesses and their directions are found as

$$\begin{aligned}\mathbf{f}_{rr} &= \begin{bmatrix} 0.9392 \\ 1.6868 \\ 0.0505 \end{bmatrix} \cdot 10^3 \text{ Nm}, \\ \Lambda_{rr} &= \begin{bmatrix} -0.9738 & 0.2272 & 0 \\ -0.2272 & -0.9738 & 0 \\ 0 & 0 & 1 \end{bmatrix}; \\ \mathbf{f}_{tt} &= \begin{bmatrix} 0.1385 \\ 0.2955 \\ 1.4229 \end{bmatrix} \cdot 10^5 \text{ N/m}, \quad \Lambda_{tt} = \begin{bmatrix} 1 & 0 & 0 \\ 0 & 1 & 0 \\ 0 & 0 & 1 \end{bmatrix}\end{aligned}\quad (35)$$

In comparison with the eigenvalues and eigenvectors in equation (32), k_ϕ , k_x and k_y become much smaller. The eigenvectors in Λ_{rr} have very small changes while Λ_{tt} is still an identity matrix, as the two parallel actuators influence k_y , k_ϕ and the third one only contribute to k_x .

Figures 6 and 7 map the principal stiffnesses over the workspace, which demonstrate the stiffness range when the manipulator stays at a prescribed pose. The map shows that the maximum values are at least 10 times higher than the minimum ones. It is found that

the rotational stiffness k_ϕ becomes higher from the left lower region of the workspace to the right boundary. The translational stiffness k_x is constant for a given y -coordinate and the manipulator becomes stiffer with the increasing y -coordinate, while k_y keeps constant for a given x -coordinate, which is associated with the partial motion decoupling of the manipulator. The overall stiffness reveals the compliance characteristics of the manipulator studied.

Experimental verification of the stiffness model

In this work, a test system was built as shown in Figure 8 for stiffness model validation. The deflection of the robot was measured via an experimental setup composed of a single Charge-Coupled Device (CCD) camera with an interface¹⁸:

- DVT 554c smart camera with 1280×1024 pixel resolution from Cognex²⁸ was fixed right above the mobile platform for pose measurements.
- INTELLECT 1.5.1, a vision software from Cognex,²⁹ was used to establish the communication with the camera via data cable.

Table 5. Details of the screw springs under external wrench.

Spring	k (N/m)	\mathbf{e}	\mathbf{p} (m)	p (rad/m)
s1	28354	$[-0.0506, -0.7158, 0.6965]^T$	$[0.0980, -0.0024, 0.0047]^T$	0.1227
s2	7010	$[-0.9885, 0.1495, 0.0218]^T$	$[0.0037, 0.0221, 0.0166]^T$	0.2145
s3	57477	$[0.0038, 0.0394, 0.9992]^T$	$[-0.0187, 0.0302, -0.0011]^T$	0.0097
s4	28354	$[0.0506, 0.7158, 0.6965]^T$	$[0.0980, -0.0024, -0.0047]^T$	-0.1227
s5	7010	$[0.9885, -0.1495, 0.0218]^T$	$[0.0037, 0.0221, -0.0166]^T$	-0.2145
s6	57477	$[0.0038, 0.0394, -0.9992]^T$	$[-0.0187, 0.0302, 0.0011]^T$	-0.0097

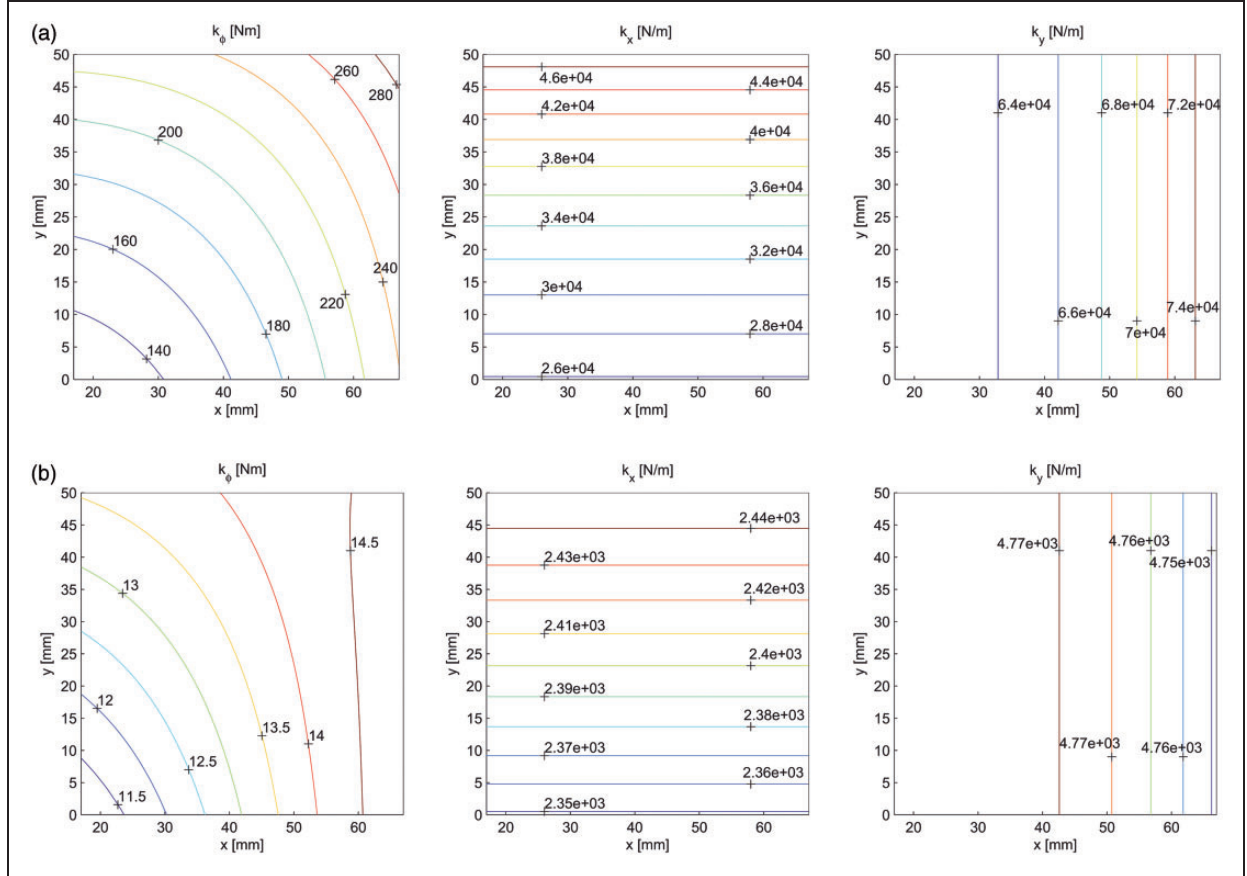


Figure 6. The overall principal stiffness with constant-orientation $\phi = 0$: (a) all the actuators at the maximum stiffness; (b) all the actuators at the minimum stiffness.

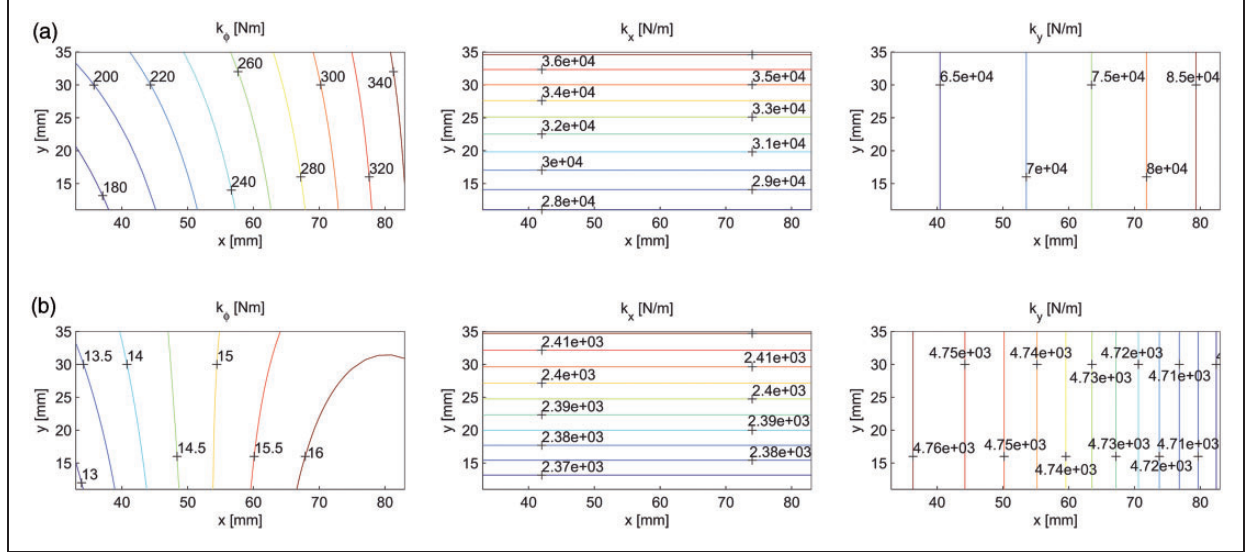


Figure 7. The principal stiffness with constant-orientation $\phi = 30^\circ$: (a) all the actuators at the maximum stiffness; (b) all the actuators at the minimum stiffness.

With this system, the position and orientation measurement accuracies are 0.01 mm and 0.01 deg, respectively. Three loading modes are applied to the mobile platform, as displayed in Figure 9: (a) planar force; (b) pure moment; (c) vertical force.

Figure 10 illustrates the comparisons between the analytical model and the experimental measurements, where the deflections are calculated from matrix of equation (22). The root-mean-square (RMS) based differences of the orientation/positioning errors

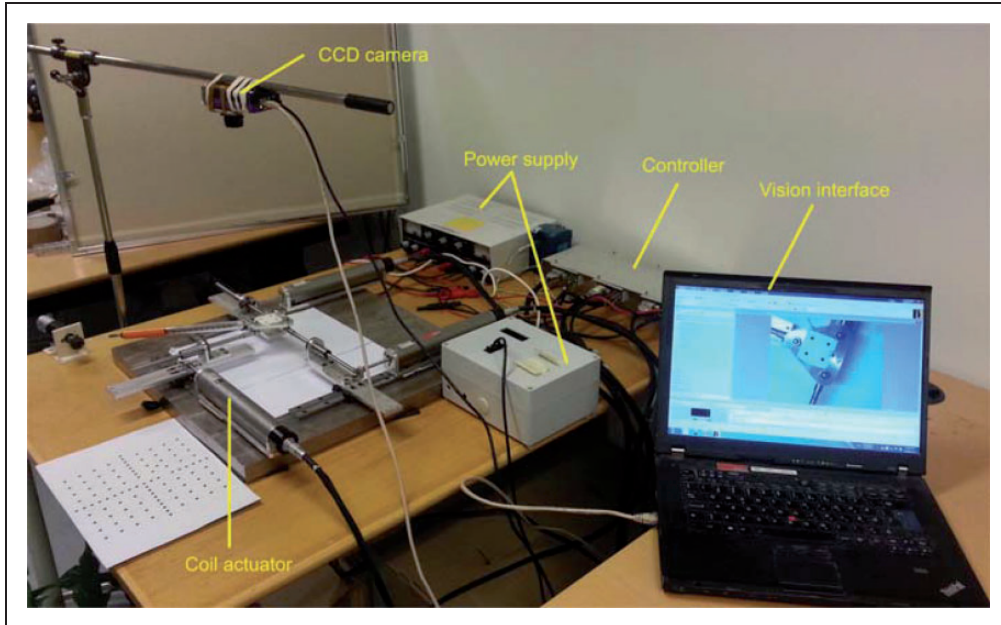


Figure 8. Vision system for the deflection measurement.

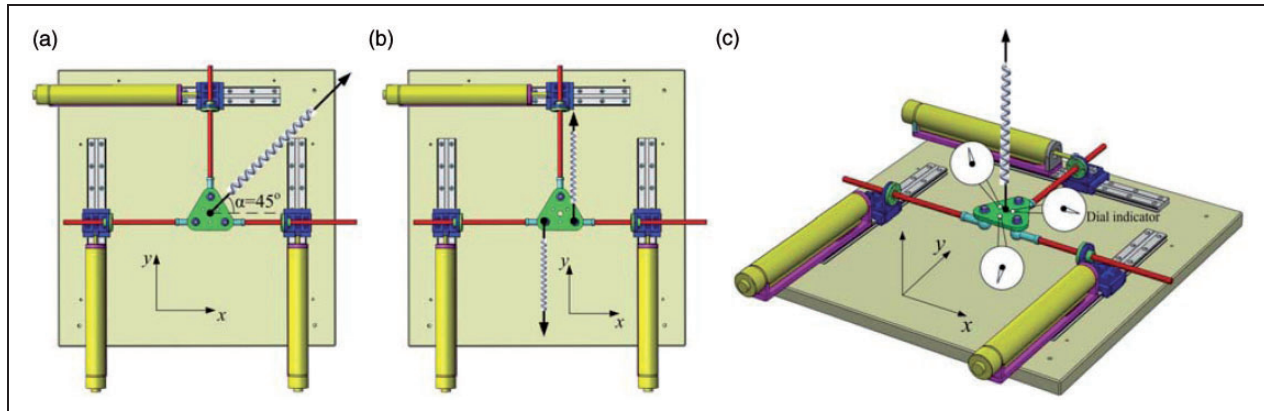


Figure 9. The three loading modes for deflection measurement: (a) planar force; (b) pure moment; (c) vertical force. In the third mode, the vertical deflection is measured by a dial indicator, to compensate the limitation of a single camera.

between the calculation and measurement are 0.089° and 0.095 mm for Figure 10(a), and the differences are 0.115° and 0.075 mm of Figure 10(b) together with 0.054 mm of Figure 10(c). One reason causing the differences is that the stiffness of the linear guides and bearing are approximated from the catalogs, and another important reason is the non-uniform friction.

Based on the comparison, it is found that the difference between the analytical model and the experimental measurements is quite small and acceptable, which means that the developed stiffness model can effectively predict the manipulator stiffness.

Conclusions

This paper addresses the problem of the stiffness modeling for compliant planar parallel manipulators with

increase modeling dimensions. This was accomplished by taking into consideration of the actuator stiffness and also the spatial deformation of the parallel manipulator. With the aid of screw theory, the generalized eigenvalue problem of the stiffness matrix, namely, the eigenscrew decomposition to compute the eigenforce, eigenpitch and eigenscrew, is investigated to interpret physical property of the stiffness matrix. A numerical method for decoupling the Cartesian stiffness matrix into two homogeneous submatrices, corresponding to the translational and rotational stiffness, is introduced. Based on decoupling of stiffness matrix, the eigenvalue problem of the two submatrices is studied separately to assess the manipulator stiffness at given configurations.

The proposed approach is applied to a 3-PPR PPM, whose actuation stiffness turns out to

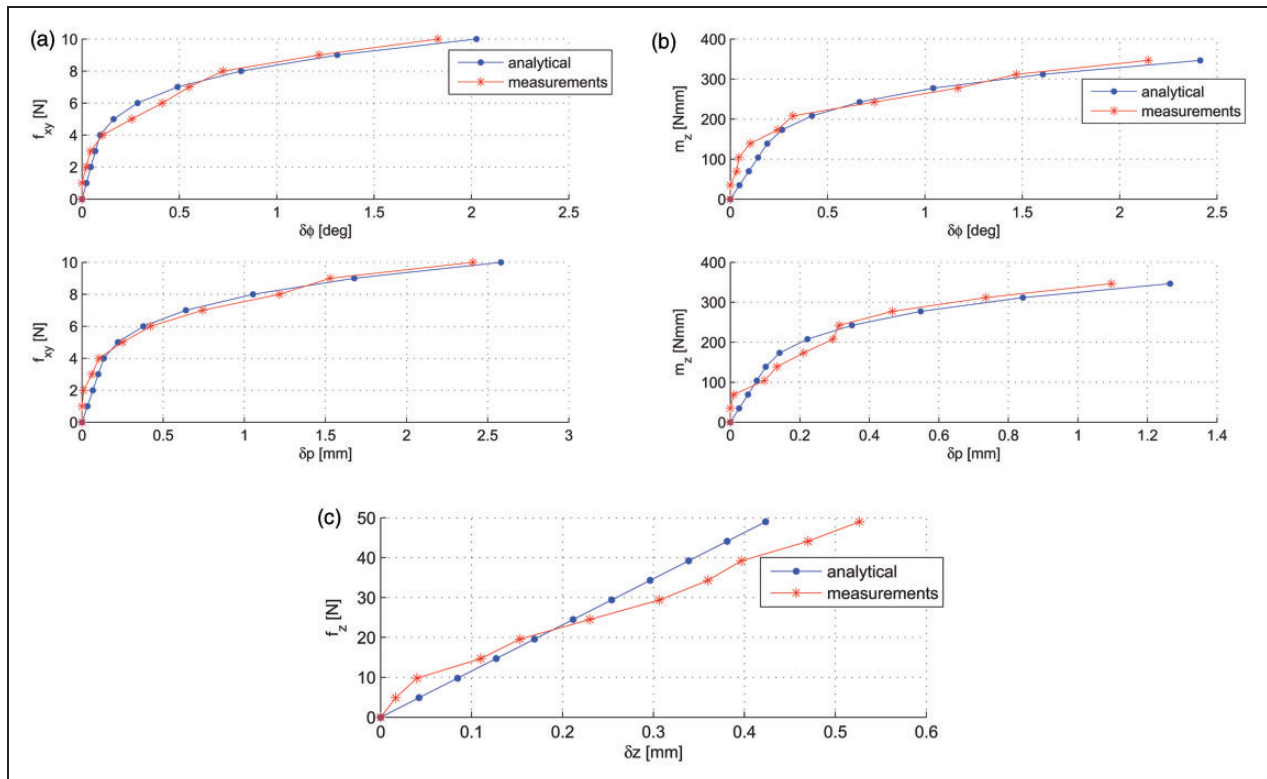


Figure 10. Comparison between analytical solutions and experimental measurements when the actuator is powered on: (a) force-displacement relation, where planar force f_{xy} along $\alpha = 45^\circ$; (b) moment (m_z)-displacement relation; (c) force (f_z)-displacement relation.

be nonlinear. Using the technique of the decoupling of stiffness matrix, the max-/minimum principal stiffness can be qualified and the corresponding directions are identified. The mappings of the principal stiffness over the workspace with constant orientations are visualized, which shows that the manipulator exhibits compliance behavior consistent with its variable actuation stiffness.

Conflict of interest

None declared.

Funding

This research received no specific grant from any funding agency in the public, commercial, or not-for-profit sectors.

References

1. Ardayfio D. *Fundamentals of robotics*. Boca Raton, Florida: CRC Press, 1987.
2. Kim WK, Lee JY and Yi BJ. Analysis for a planar 3 degree-of-freedom parallel mechanism with actively adjustable stiffness characteristics. *IEEE Int Conf Rob Autom* 1997; 3: 2663–2670.
3. Kock S and Schumacher W. A parallel $x-y$ manipulator with actuation redundancy for high-speed and active-stiffness applications. *IEEE Int Conf Rob Autom* 1998; 3: 2295–2300.
4. Lee S, Kim S, In W, et al. Experimental verification of antagonistic stiffness planning for a planar parallel mechanism with 2-DOF force redundancy. *Robotica* 2011; 29: 547–554.
5. Zhao TS, Zhao YZ, Shi LJ, et al. Stiffness characteristics and kinematics analysis of parallel 3-DOF mechanism with flexible joints. *Int Conf Mechatron Autom* 2007; 1822–1827.
6. Alici G and Shirinzadeh B. Kinematics and stiffness analyses of a flexure-jointed planar micromanipulation system for a decoupled compliant motion. *IEEE/RSJ Int Conf Intell Rob Syst* 2003; 4: 3282–3287.
7. Yi BJ, Chung GB, Na HY, et al. Design and experiment of a 3-DOF parallel micromechanism utilizing flexure hinges. *IEEE Int Conf Rob Autom* 2003; 19: 604–612.
8. Kang BH, Ting-Yung Wen J, Dagalakis NG, et al. Analysis and design of parallel mechanisms with flexure joints. *IEEE Trans Rob* 2005; 21: 1179–1185.
9. Li Y and Xu Q. Design and analysis of a totally decoupled flexure-based XY parallel micromanipulator. *IEEE Trans Rob* 2009; 25: 645–657.
10. Bhagat U, Shirinzadeh B, Clark L, et al. Design and analysis of a novel flexure-based 3-DOF mechanism. *Mech Mach Theory* 2014; 74: 173–187.
11. Ciblak N and Lipkin H. Synthesis of Cartesian stiffness for robotic applications. *IEEE Int Conf Rob Autom* 1999; 3: 2147–2152.
12. Ding X and Selig JM. On the compliance of coiled springs. *Int J Mech Sci* 2004; 46: 703–727.
13. Dai J and Ding X. Compliance analysis of a three-legged rigidly-connected platform device. *J Mech Des* 2006; 128: 755–764.

14. Kövecses J and Ebrahimi S. Parameter analysis and normalization for the dynamics and design of multi-body systems. *J Comput Nonlinear Dyn* 2009; 4: 031008(1–10).
15. Taghvaeipour A, Angeles J and Lessard L. On the elastostatic analysis of mechanical systems. *Mech Mach Theory* 2012; 58: 202–216.
16. Angeles J. On the nature of the Cartesian stiffness matrix. *Ingeniería Mecánica* 2010; 3: 163–170.
17. Bai S and Caro S. Design and analysis of a 3-PPR planar robot with U-shape base. *Int Conf Adv Rob* 2009; 1–6.
18. Wu G, Bai S, Kepler J, et al. Error modeling and experimental validation of a planar 3-PPR parallel manipulator with joint clearances. *J Mech Rob* 2012; 4: 041008(1–12).
19. Pashkevich A, Chablat D and Wenger P. Stiffness analysis of overconstrained parallel manipulators. *Mech Mach Theory* 2009; 44: 966–982.
20. Wu G, Bai S and Kepler J. Mobile platform center shift in spherical parallel manipulators with flexible limbs. *Mech Mach Theory* 2014; 75: 12–26.
21. Ball RS. *A treatise on the theory of screws*. Cambridge, England: Cambridge University Press, 1900.
22. Huang S and Schimmels JM. The eigenscrew decomposition of spatial stiffness matrices. *IEEE Trans Rob Autom* 2000; 16: 146–156.
23. Pradeep AK, Yoder PJ and Mukundan R. On the use of dual-matrix exponentials in robotic kinematics. *Int J of Rob Res* 1989; 8: 57–66.
24. Angeles J. *Fundamentals of robotic mechanical systems: theory, methods, and algorithms*. New York: Springer, 2007.
25. Roberts RG. On the normal form of a spatial stiffness matrix. *Proc IEEE Int Conf Rob Autom* 2002; 1: 556–561.
26. Strang G. *Linear algebra and its applications*. 4th ed. Boston, Massachusetts: Cengage Learning, 2005.
27. Russell D and Rossing T. Testing the nonlinearity of piano hammers using residual shock spectra. *Acta Acustica United Acustica* 1998; 85: 967–975.
28. <http://www.pdfsupply.com/pdfs/dvt-554c.pdf>.
29. <http://www.cognex.com/support/downloads/File.aspx?d=643>.

Appendix

The Jacobians in equation (1) are given as

$$\begin{aligned} \mathbf{J}_\rho^i &= \widehat{\$}_\rho^i; & \mathbf{J}_q^i &= \begin{bmatrix} \widehat{\$}_C^i & \widehat{\$}_l^i & \widehat{\$}_D^i \end{bmatrix}; \\ \mathbf{J}_\theta^i &= \begin{bmatrix} \mathbf{J}_g^i & \mathbf{J}_s^i & \mathbf{J}_b^i & \mathbf{J}_l^i \end{bmatrix} \end{aligned} \quad (36)$$

with

$$\begin{aligned} \mathbf{J}_g^i &= \begin{bmatrix} \widehat{\$}_{g1}^i & \dots & \widehat{\$}_{g6}^i \end{bmatrix}; & \mathbf{J}_s^i &= \begin{bmatrix} \widehat{\$}_{s1}^i & \dots & \widehat{\$}_{s6}^i \end{bmatrix}; \\ \mathbf{J}_b^i &= \begin{bmatrix} \widehat{\$}_{b1}^i & \dots & \widehat{\$}_{b4}^i \end{bmatrix}; & \mathbf{J}_l^i &= \begin{bmatrix} \widehat{\$}_{l1}^i & \dots & \widehat{\$}_{l6}^i \end{bmatrix} \end{aligned} \quad (37)$$

where the unit screws are given below

$$\begin{aligned} \widehat{\$}_\rho^i &= \begin{bmatrix} \mathbf{0} \\ \mathbf{u}_i \end{bmatrix}, \quad \widehat{\$}_C^i = \begin{bmatrix} \mathbf{w}_i \\ \mathbf{c}_i \times \mathbf{w}_i \end{bmatrix}, \quad \widehat{\$}_l^i = \begin{bmatrix} \mathbf{0} \\ \mathbf{w}_i \end{bmatrix}, \\ \widehat{\$}_D^i &= \begin{bmatrix} \mathbf{k} \\ \mathbf{d}_i \times \mathbf{k} \end{bmatrix} \\ \widehat{\$}_{g1}^i &= \begin{bmatrix} \mathbf{u}_i \\ \mathbf{b}_i \times \mathbf{u}_i \end{bmatrix}, \quad \widehat{\$}_{g2}^i = \begin{bmatrix} \mathbf{y}_{iB} \\ \mathbf{b}_i \times \mathbf{y}_{iB} \end{bmatrix}, \quad \widehat{\$}_{g3}^i = \begin{bmatrix} \mathbf{k} \\ \mathbf{b}_i \times \mathbf{k} \end{bmatrix}, \\ \widehat{\$}_{g4}^i &= \begin{bmatrix} \mathbf{0} \\ \mathbf{y}_{iB} \end{bmatrix}, \quad \widehat{\$}_{g5}^i = \begin{bmatrix} \mathbf{0} \\ \mathbf{k} \end{bmatrix} \\ \widehat{\$}_{s1}^i &= \begin{bmatrix} \mathbf{v}_i \\ \mathbf{c}_i \times \mathbf{v}_i \end{bmatrix}, \quad \widehat{\$}_{s2}^i = \begin{bmatrix} \mathbf{y}_{iC} \\ \mathbf{c}_i \times \mathbf{y}_{iC} \end{bmatrix}, \quad \widehat{\$}_{s3}^i = \begin{bmatrix} \mathbf{k} \\ \mathbf{c}_i \times \mathbf{k} \end{bmatrix}, \\ \widehat{\$}_{s4}^i &= \begin{bmatrix} \mathbf{0} \\ \mathbf{v}_i \end{bmatrix}, \quad \widehat{\$}_{s5}^i = \begin{bmatrix} \mathbf{0} \\ \mathbf{y}_{iC} \end{bmatrix}, \quad \widehat{\$}_{s6}^i = \begin{bmatrix} \mathbf{0} \\ \mathbf{k} \end{bmatrix} \\ \widehat{\$}_{b1}^i &= \begin{bmatrix} \mathbf{y}_{iD} \\ \mathbf{c}_i \times \mathbf{y}_{iD} \end{bmatrix}, \quad \widehat{\$}_{b2}^i = \begin{bmatrix} \mathbf{k} \\ \mathbf{c}_i \times \mathbf{k} \end{bmatrix}, \quad \widehat{\$}_{b3}^i = \begin{bmatrix} \mathbf{0} \\ \mathbf{y}_{iD} \end{bmatrix}, \\ \widehat{\$}_{b4}^i &= \begin{bmatrix} \mathbf{0} \\ \mathbf{k} \end{bmatrix} \\ \widehat{\$}_{l1}^i &= \begin{bmatrix} \mathbf{w}_i \\ \mathbf{d}_i \times \mathbf{w}_i \end{bmatrix}, \quad \widehat{\$}_{l2}^i = \begin{bmatrix} \mathbf{y}_{iD} \\ \mathbf{d}_i \times \mathbf{y}_{iD} \end{bmatrix}, \\ \widehat{\$}_{l3}^i &= \widehat{\$}_{iD}, \quad \widehat{\$}_{l4}^i = \begin{bmatrix} \mathbf{0} \\ \mathbf{w}_i \end{bmatrix}, \quad \widehat{\$}_{l5}^i = \begin{bmatrix} \mathbf{0} \\ \mathbf{y}_{iD} \end{bmatrix}, \quad \widehat{\$}_{l6}^i = \begin{bmatrix} \mathbf{0} \\ \mathbf{k} \end{bmatrix} \end{aligned} \quad (38)$$

where \mathbf{b}_i , \mathbf{c}_i and \mathbf{d}_i are position vectors of points B_i , C_i and D_i from point P , respectively, while \mathbf{k} is the unit vector of z -axis, and

$$\mathbf{y}_{iB} = \frac{\mathbf{k} \times \mathbf{u}_i}{\|\mathbf{k} \times \mathbf{u}_i\|}, \quad \mathbf{y}_{iC} = \frac{\mathbf{k} \times \mathbf{v}_i}{\|\mathbf{k} \times \mathbf{v}_i\|}, \quad \mathbf{y}_{iD} = \frac{\mathbf{k} \times \mathbf{w}_i}{\|\mathbf{k} \times \mathbf{w}_i\|} \quad (39)$$